Physics of Living Systems

Interplay of condensate material properties and chromatin heterogeneity governs nuclear condensate ripening

Reviewed Preprint
v1 • November 27, 2024
Not revised

Deb Sankar Banerjee, Tafadzwa Chigumira, Rachel M Lackner, Josiah C Kratz, David M Chenoweth, Shiladitya Banerjee, Huaiying Zhang

Department of Physics, Carnegie Mellon University, Pittsburgh, PA 15213, USA • James Franck Institute, University of Chicago, Chicago, USA • Department of Chemical Engineering, Carnegie Mellon University, Pittsburgh, USA • Department of Chemistry, University of Pennsylvania, Philadelphia, USA • Department of Biological Sciences, Carnegie Mellon University, Pittsburgh, USA • Computational Biology Department, Carnegie Mellon University, Pittsburgh, USA

eLife Assessment

In this potentially **valuable** study, the authors employed in vivo experiments and theoretical modeling to study the growth dynamics of nuclear condensates. They observed that condensates can exhibit distinct growth modes, as dictated by the competition between condensate surface tension and local elasticity of chromatin. While the theoretical model appears to capture the experimental observations, the level of evidence supporting the proposed growth mechanism is **incomplete** due to, among other limitations, the multiple fitting parameters and poorly justified Neo-Hookean elasticity.

https://doi.org/10.7554/eLife.101777.1.sa2

Abstract

Nuclear condensates play many important roles in chromatin functions, but how cells regulate their nucleation and growth within the complex nuclear environment is not well understood. Here, we report how condensate properties and chromatin mechanics dictate condensate growth dynamics in the nucleus. We induced condensates with distinct properties using different proteins in human cell nuclei and monitored their growth. We revealed two key physical mechanisms that underlie droplet growth: diffusion-driven or ripening-dominated growth. To explain the experimental observations, we developed a quantitative theory that uncovers the mechanical role of chromatin and condensate material properties in regulating condensate growth in a heterogeneous environment. By fitting our theory to experimental data, we find that condensate surface tension is critical in determining whether condensates undergo elastic or Ostwald ripening. Our model also predicts that chromatin heterogeneity can influence condensate nucleation and growth, which we validated by experimentally perturbing the chromatin organization and controlling condensate

nucleation. By combining quantitative experimentation with theoretical modeling, our work elucidates how condensate surface tension and chromatin heterogeneity govern nuclear condensate ripening, implying that cells can control both condensate properties and the chromatin organization to regulate condensate growth in the nucleus.

Introduction

The human cell nucleus is a complex environment containing various nuclear bodies embedded in or attached to an expansive network of chromatin (1). These nuclear bodies, such as the nucleoli, histone locus body, PML bodies, and DNA-damage foci, play important roles in facilitating chromatin functions such as transcription, replication and DNA repair (2, 3). There is increasing evidence that nuclear bodies are biomolecular condensates formed by phase separation (4–7). Given the intrinsic ability of the liquid-like condensates to coarsen via coalescence and Ostwald ripening (8), how cells regulate these processes to achieve controlled growth at sites of nucleation become an outstanding question. This question is particularly important for nuclear condensates as many of their chromatin associated functions depend on proper localization (9, 10).

Previous works have shown that the stiffness of the chromatin network can inhibit condensate nucleation (11). In addition, chromatin can inhibit condensate coalescence by reducing condensate mobility and prevent Ostwald ripening by suppressing the growth of large condensates (12, 13). These studies suggest that cells can potentially regulate local chromatin stiffness to control condensate growth in the nucleus.

However, the role of the chromatin organization is less clear. Chromatin is not uniformly distributed in the nucleus but known to have a heterogeneous organization where heterochromatin domains are more dense while the euchromatin regions are less dense (14, 15). This variability in density is additionally regulated by cells, effectively controlling access to genes and influencing nuclear body function and location (2, 3). Chromatin organization goes awry in diseased cells, which may contribute to the aberrant condensate landscape (16, 17). Heterogeneity in chromatin density correlates with heterogeneity in mechanical stiffness, but how this mechanical heterogeneity affects condensate nucleation and growth remains to be learned.

In addition to the chromatin, the condensate properties can also be important in controlling the formation and growth of nuclear condensates. Theory and experiments in colloidal systems revealed that liquid droplets can grow in a polymer network if the condensation pressure is larger than the elastic forces from the polymer (18). On the other hand, gradients in stiffness can inhibit Ostwald ripening or drive elastic ripening, depending on the relative strength of stiffness gradient to surface tension (19). This suggests that cells potentially regulate both chromatin stiffness and condensate properties to control condensate growth in the chromatin. Biomolecular condensates are known to have a wide range of material properties such as surface tension and viscosity (20). However, it is not known whether surface tension of nuclear condensates can be in the range to counter the influence of chromatin stiffness and thus can be exploited by cells to fine-tune condensate nucleation, growth, and sizes in the nucleus.

In this work, we address these outstanding questions by using a chemical dimerizer to induce two types of nuclear condensates in different chromatin environments for comparative growth dynamics assessment. We observe that both types of condensates can grow through coalescence, diffusion, and ripening. However, the proportions of each growth mode are different for the different types of condensates. To explain the experimental observations, we developed a physical model for condensate growth in a heterogeneous elastic environment that represent the chromatin network. In particular, we considered the effect of size-dependent mechanical pressures that condensates may experience from the surrounding chromatin. Our model captures

the experimentally measured condensate growth dynamics and predicts the stability of condensates based on their surface tension and the surrounding chromatin stiffness. The model predicts that the coarsening dynamics for different condensates are affected differently by changes in the chromatin landscape, which we confirmed experimentally by perturbing the heterogeneity in chromatin organization. Together, our work shows that the interplay between condensate surface tension and chromatin mechanical heterogeneity controls condensate growth in the heterogeneous physical environment of the nucleus. This indicates that cells can regulate both the material properties and the chromatin organization to control condensate growth, and the aberrant nuclear condensate landscape in diseased cells can be attributed to abnormality in condensate composition and chromatin organization.

Results

Condensates made with different proteins have different material properties

To test whether condensate material properties affect condensate growth in the nucleus, we selected a coiled-coil protein and a disordered protein to generate condensates that we predicted to have different material properties. For the coiled-coil protein, we chose Mad1, a human mitotic protein that has the propensity to form condensates (21). For the disordered protein, we chose the intrinsically disordered region of the *C. elegans* p-granule protein LAF-1 that is rich in arginine-glycine-glycine (RGG) repeats (22). We used a previously described chemical dimerization system to induce condensates by linking the phase separation proteins to an oligomer in the nucleus of U2OS cells (23–25) (**Fig. 1A**). The dimerizer Trimethoprim-Fluorobenzamide-Halo ligand (TFH), consisting of chemically linked Trimethoprim and a Halo-ligand that interact with eDHFR and Halo enzyme, respectively, can dimerize proteins fused to eDFHR and Halo (26) (**Fig. 1A**). Using THF to dimerize LacI, a dimer protein, to Mad1 was enough to initiate the coiled-coil condensate formation (Movie 1). A hexamer, Hotag3 (25), was required to be dimerized to RGG to induce the disordered condensates in the nucleus (Movie 2).

Having successfully induced two types of nuclear condensates, we tested whether their physical properties were significantly different. First, we estimated the partition coefficients by calculating the ratio of the mean fluorescent intensity in the condensed phase to the dilute phase. We found the partition coefficient of the disordered protein condensate to be half of that of the coiled-coil protein condensate, implying that the coiled-coil domains make for condensates with greater internal interaction strength than the disordered condensates (27) (**Fig. 1B**).

Next, we performed fluorescence recovery after photobleaching (FRAP) at the center of the condensates to compare the difference in viscosities, η, between the two condensates (22) (**Fig. 1C,D**). Exponential fits to the intensity recovery curves yield the recovery time τ, which for the coiled-coil condensate is in the order of minutes and that for the disordered condensate is in the order of seconds, suggesting that the two types of condensates exhibit significantly different dynamics (28) (**Fig. 1C,D** inserts). By combining $D \sim r^2/\tau$, where r is bleached spot radius, with the Stokes-Einstein relation $D = k_B T/6\pi\eta a$, where k_B is the Boltzmann constant, T is temperature, η is the viscosity, and a is the hydrodynamic radius of the diffusing particles that were assumed to scale linearly with the molecular weights of the phase separation proteins, we estimated that the coiled-coil condensate has a viscosity, η, 33 times larger than that of the disordered condensate (**Fig. 1B**).

We then used droplet fusion assays (4, 22, 28) to estimate the difference in surface tension, γ, of these two condensates. Similar to FRAP recovery, coiled-coil condensates take significantly longer time to round up during fusion (**Fig. 1E,F**). By assuming η/γ scales linearly with τ/r (4),

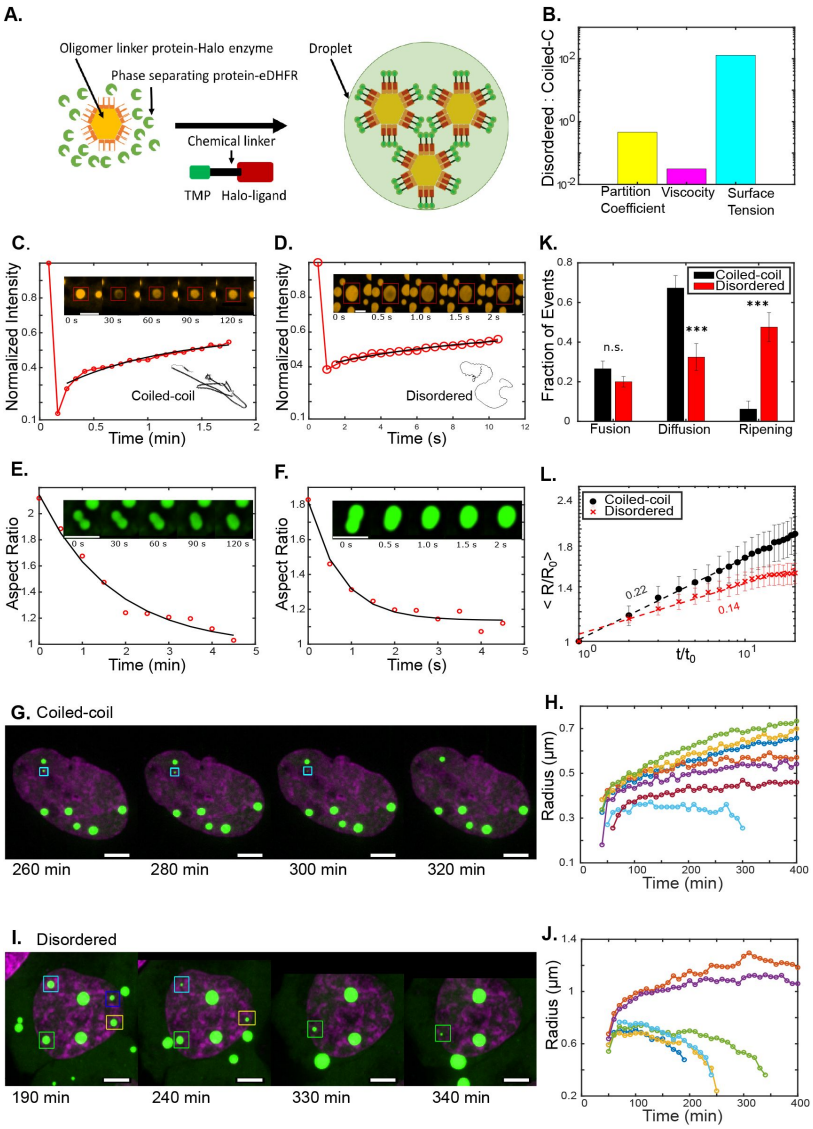

Fig. 1.

Condensates with different properties have significantly different growth patterns and coarsening kinetics.

(A) A schematic for the use of a chemical dimerizer to induce condensate formation. (B) The ratio of the disordered protein condensate partition coefficient, viscosity, and surface tension to the coiled-coil condensate. (C,D) FRAP images and curves for a coiled-coil protein condensate (in C) and a disordered protein condensate (in D). Black lines are the exponential fits. Inset schematics are the predicted structure of the coiled-coil Mad1 protein (in C) and the disordered RGG domain of LAF-1 protein (in D) from AlphaFold2. (E,F) Fusion images and plots of aspect ratio over time for coiled-coil condensates (in E) and discorded protein condensates (in F). Black lines are the exponential fits. (G) Representative U2OS cell nucleus (magenta with DNA staining) containing condensates (green) formed by the coiled-coil protein imaged over time. Box indicates condensate that shrinks. (H) Condensate radius vs time for the six coiled-coil protein condensates shown in G. (I) Representative U2OS cell nucleus (magenta with DNA staining) containing disordered protein condensates (green) imaged over time. Boxes indicate condensates that shrink over time. (J) Condensate radius vs time for the six disordered condensates shown in I. (K) Fraction of growth types of the coiled-coil and the disordered protein condensates. Fusion events were scored as the coalescence of condensates, ripening events are characterized as the number of condensates shrinking while the remaining condensates grow, and diffusion-based growth is scored as continuous growth in the absence of ripening and can occur alongside fusion events (n.s., no significance; ***, p<0.001). (L) Change of average condensate radii over time. Condensate radius was normalized to the average condensate size at nucleation and time is normalized to the time nucleation occurs in the cell. Dashed lines are linear fits yielding indicated slopes. Scale bar, 5 μm.

where r is the length of the fusing condensates, and τ is the relaxation time obtained by using exponential fit of the relaxation curves, we estimated the surface tension, γ, for the disordered condensates to be 130 times greater than the coil-coil condensates (**Fig. 1B**).

Taken together, these analyses show that condensates formed with coiled-coil and disordered proteins have distinct material properties including viscosity and surface tension.

Coiled-coil condensates and disordered condensates exhibit significantly different growth dynamics

Having confirmed the distinct properties of these two types of condensates, we proceeded to follow condensate coarsening dynamics. By using confocal microscopy to follow the condensates over time (**Fig. 1G, I**, Movie 1, 2) and by plotting the size of each condensate over time (**Fig. 1H, J**), we observed three modes of condensate coarsening: fusion, ripening, and continuous diffusion based growth, for both the coiled-coil and the disordered condensates (**Fig. 1H,J**).

By defining fusion as when two condensates coalesce to form a larger one, ripening as the shrinkage of condensates, and diffusion-based growth as continuous growth in the absence of ripening, we quantified the fraction of the different growth events by condensate type and observed significantly different growth patterns for the two condensates (**Fig. 1K**). First, ripening accounted for the majority of the growth events in disordered condensates compared to the least fraction in the coiled-coil condensates (**Fig. 1K**). In addition, the ripening time, defined as the time taken for a condensate to shrink over its radius, was 200 min/μm for the disordered condensates and 1100 min/μm for the coiled-coil condensates (Fig. S1). This suggests not only a greater ripening propensity for the disordered condensates but also faster ripening rates. Second, diffusion-based growth accounts for majority of growth for the coiled-coil condensates (67% of growth events) but it is only a small fraction for the disordered condensates (32% of growth events) (**Fig. 1K**). Lastly, growth by fusion for the disordered protein (20% of growth events) was similar to that of the coiled-coil condensate (27% of growth events) (**Fig. 1K**). Moreover, these growth patterns are also different from that reported for the FUS protein condensates where condensates grow dominantly by fusion while ripening and longer-term diffusion-based growth are absent (29, 30). These results suggest that condensate properties can affect the condensate growth patterns.

To assess the effect of condensate properties on coarsening rates, we plotted the average normalized condensate radius $\langle R/R_0 \rangle$ over time t (**Fig. 1L**). A power law fit following $\langle R \rangle \sim t^{\beta}$, where β is the growth exponent, yielded $\beta = 0.22$ for the coiled-coil condensates and $\beta = 0.14$ for the disordered condensate (**Fig. 1L**). Both exponents are smaller than predicted by theory (1/2 for diffusion based growth and 1/3 for fusion and ripening based growth) and are closer, even though still different from, the $\beta = 0.12$ observed for the FUS protein condensates (29). Given that the coiled-coil condensates and the disordered condensates had similar opportunities to grow by fusion but had different growth exponents (**Fig. 1K, L**), we suspect that their growth suppression may be attributed to the effect of chromatin on ripening or diffusion-based growth, different from the suppression of condensate fusion by chromatin for FUS condensates (29).

Together these results show that condensate growth is generally suppressed in the nucleus, but different condensates could be affected differently, likely due to different interplay between the condensates properties and the chromatin mechanics.

Theoretical model of condensate growth in heterogeneous elastic media

To quantitatively understand how the different growth patterns emerge from the interplay between the condensate materials properties and the mechanics of the surrounding chromatin network, we developed a theory of condensate growth in elastic media (**Fig. 2A**-inset). Using the condition of material flux balance in and out of the condensate, we can formulate the growth dynamics of a spherical condensate in terms of its radius R as (31–33):

$$\frac{\mathrm{d}R}{\mathrm{d}t} = \frac{D}{Rc_{\mathrm{in}}}\left(c_{\infty} - c_{\mathrm{out}}\right) \qquad \textbf{(1)}$$

where D is the diffusion constant for the proteins in the dilute phase, c_{∞} is the far field concentration of the dilute phase, c_{in} and c_{out} are the concentrations of the proteins inside and outside the condensate. Considering the mass conservation of the total amount of condensate forming proteins and the effect of local pressure P on the dilute phase concentration, we arrive at (see Supplementary Materials Sec I for derivation):

$$\frac{\mathrm{d}R}{\mathrm{d}t} = \frac{D}{Rc_{\mathrm{in}}}\left(\bar{c} - c_{\mathrm{in}}\frac{4\pi R^3}{3V} - c^0_{\mathrm{out}}\exp\left[\frac{P(R)}{c_{\mathrm{in}}k_BT}\right]\right), \qquad \textbf{(2)}$$

where $\bar{c}$ is the average protein concentration, c^0_{out} is the equilibrium protein concentration outside the droplet, V is the volume of the nucleus, and T is the temperature. Surface tension (γ) of the condensates and local stiffness of the chromatin network (E) both contribute to the condensate size-dependent pressure:

$$P(R) = \frac{2\gamma}{R} + P_E(R) \qquad \textbf{(3)}$$

where P_E the pressure due to elastic deformation of the chromatin network. It has been suggested that chromatin networks exhibit hyper-elasticity due to their nonlinear stress-strain relationship (12, 34, 35). Consequently, we adopted a form for the mechanical pressure P_E derived from the known material response during the expansion of a cavity, created by condensate growth in a neo-Hookean elastic solid (36). This yields $P_E(R) = E\left(\frac{5}{6} - \frac{2\xi}{3R} - \frac{\xi^4}{6R^4}\right)$, where ξ is the mesh size of the chromatin network surrounding the condensate.

The pressure P_E is zero when the condensate size is smaller than the mesh size ($R < \xi$).

Given the chromatin network is mechanically heterogeneous, its mesh size ξ and stiffness E are assumed to be local parameters (i.e., parameter value depends on the location of the condensate). On the other hand, condensate surface tension, diffusion constant, and the concentration values are assumed to be the same for all condensates within the nucleus. Properties of the condensate forming proteins and their molecular interactions determine the values of the parameters γ, D, c_{in}, $\bar{c}$ and c^0_{out}. For N condensates growing in a shared environment, the growth dynamics for the i^{th} condensate can be written as:

$$\frac{\mathrm{d}R_i}{\mathrm{d}t} = \frac{D}{R_i c_{\mathrm{in}}}\left(\bar{c} - c_{\mathrm{in}}\frac{4\pi}{3V}\sum_{j=1}^{N} R_j^3 - c^0_{\mathrm{out}}\exp\left[\frac{P_i(R_i)}{c_{\mathrm{in}}k_BT}\right]\right), \qquad \textbf{(4)}$$

where R_i is the size of the i^{th} condensate, and P_i is the local pressure around the i^{th} condensate with stiffness E_i and mesh size ξ_i.

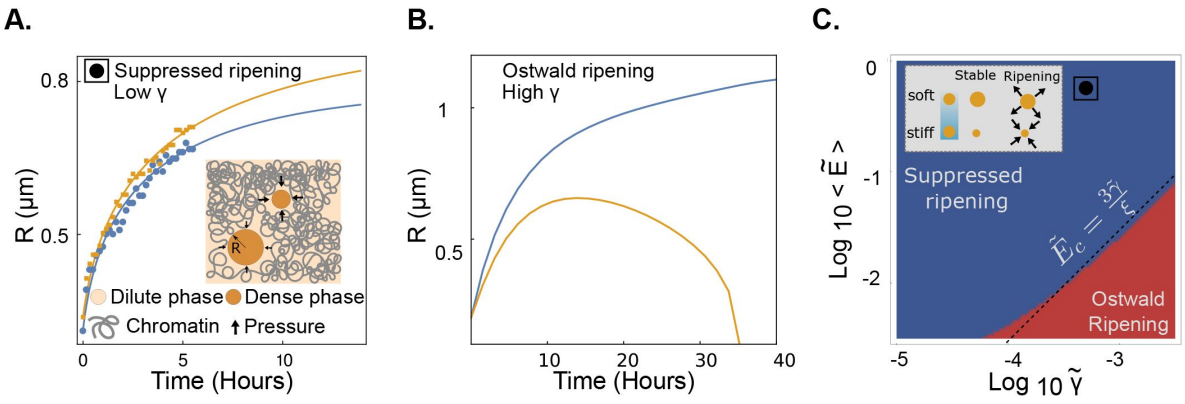

Fig. 2.

Distinct growth patterns emerge from the interplay between condensate surface tension and stiffness of the chromatin network.

(A) Radii vs time for two condensates (labelled in yellow and blue) undergoing diffusive growth (suppressed ripening). The solid lines indicate model fits (see Methods for details) to the experimental data (solid circles). (B) Radii vs time for two condensates (labelled in yellow and blue) undergoing Ostwald ripening. Here the condensates have a larger surface tension compared to (A), with all other parameters fixed. (C) Phase diagram for condensate growth behavior as a function of normalized mean stiffness $\langle \tilde{E} \rangle = (E_1 + E_2)/(2c_{\text{in}}k_BT)$ and surface tension $\tilde{\gamma} = \gamma/(c_{\text{in}}k_BT)$, showing regimes of diffusive growth (stable) and Ostwald ripening. The parameter values used for panel A and B are $D\bar{c}/c_{\text{in}} = 0.001$, $4\pi D/3V = 10^{-5}\ \mu\text{m}^{-1}\ \text{s}^{-1}$, $\langle \tilde{E} \rangle = 0.3$, $\langle \Delta\tilde{E} \rangle = 0.001$, $\xi = 0.05\mu\text{m}$ and the renormalized surface tension values are $\tilde{\gamma} = 5 \times 10^{-4}\ \mu\text{m}$ for panel A and $\tilde{\gamma} = 10^{-2}\ \mu\text{m}$ for panel B. For panel C the values are $D\bar{c}/c_{\text{in}} = 0.0008\ \mu\text{m}^2\text{s}^{-1}$ and $Dc^0_{\text{out}}/c_{\text{in}} = 0.0005$ and other relevant parameters are same as in panel A & B.

Model reveals the relative roles of surface tension and chromatin elasticity on condensate growth dynamics

We first consider the growth of two condensates of radii R_1 and R_2, embedded in the chromatin network with local stiffness values E_1 and E_2, respectively. This simplified two-droplet model is useful to elucidate the underlying mechanism of condensate ripening and its suppression, regulated by the interplay between droplet surface tension and chromatin stiffness. We used the growth model (Eq. 4) to fit experimental data from coiled-coil condensates showing suppressed ripening (**Fig. 2A**). Details of the fitting method is provided in the Methods section. Theoretical results show that the condensates can undergo Ostwald ripening when the surface tension is increased keeping all other parameters and the stiffness of the surrounding elastic medium the same (**Fig. 2B**). This explains the increased ripening of the disordered condensates (**Fig. 1K**) that have a higher surface tension compared to the coiled-coil condensates (**Fig. 1B**), with the latter exhibiting mostly diffusive growth (**Fig. 1K**). The theoretically obtained phase diagram in the plane of renormalized average stiffness $\langle\tilde{E}\rangle = (E_1 + E_2)/(2c_{\text{in}}k_BT)$) and surface tension $\tilde{\gamma} = \gamma/(c_{\text{in}}k_BT)$, with a fixed stiffness difference $\Delta\tilde{E} = (E_1 - E_2)/(c_{\text{in}}k_BT)$, shows the parameter regimes of suppressed ripening and Ostwald ripening phases, indicating that protein property $(\tilde{\gamma})$ and the mechanical property of the chromatin network $(\langle\tilde{E}\rangle)$ can determine the resulting condensate growth dynamics (**Fig. 2C**).

Condensate material properties and chromatin heterogeneity determine the modes of ripening

The low surface tension in coiled-coil condensates precludes Ostwald ripening as the mechanical pressure from the surrounding elastic network will stabilize the ripening droplets at different sizes (Fig S1, **Fig. 2A**). However, we observed a small fraction of coiled-coil condensates undergoing ripening in the elastic chromatin network (**Fig. 1G,H&K**). Recent studies on oil droplets in silica gel have shown that droplets can undergo elastic ripening due to differences in mechanical pressure from the surrounding medium (37). However, to the best of our knowledge, no instances of elastic ripening have been reported in living cells. The fitting of our model to the experimental data of ripening in coiled-coil condensates indicates a significant difference in local stiffness values which might be enough to drive elastic ripening of the coiled-coil condensates (Fig S2).

To investigate the underlying mechanism of condensate ripening in the chromatin network with spatially heterogeneous mechanical properties, we derived a linearized theory for the dynamics of the droplet size difference ΔR given by:

$$\frac{\mathrm{d}\Delta R}{\mathrm{d}t} \approx \frac{c}{R}\left[\left(2\tilde{\gamma} - \frac{2\xi}{3}\langle\tilde{E}\rangle\right)\frac{\Delta R}{R^2} + \left(\frac{5}{6} - \frac{2\xi}{3R}\right)\Delta\tilde{E}\right], \quad \textbf{(5)}$$

where R is the typical condensate size (see Supplementary Materials Sec II for details). The linearized theory is valid when ΔR is small, such that $R_1 \sim R_2 \sim R$, and is useful to derive the condition for the onset of ripening. Stability analysis of Eq. 5 reveals three distinct modes of condensate coarsening. For large enough surface tension $\tilde{\gamma} > \xi\langle\tilde{E}\rangle/3$, ΔR increases over time, leading to the growth of the larger condensate at the expense of the smaller one, suggestive of Ostwald ripening (**Fig. 3A**). This is comparable to the disordered condensates in our experiments that possess high surface tension and exhibit Ostwald ripening (**Fig. 1K,L**). By contrast, when $\langle\tilde{E}\rangle > 3\tilde{\gamma}/\xi$, Ostwald ripening is suppressed by the mechanical pressure from the surrounding chromatin network, leading to a stable size difference between the condensates $\Delta R^* = \Delta E(5R - 4\xi)R/(12(\frac{\xi\langle\tilde{E}\rangle}{3} - \tilde{\gamma}))$ (see **Fig. 3A**).

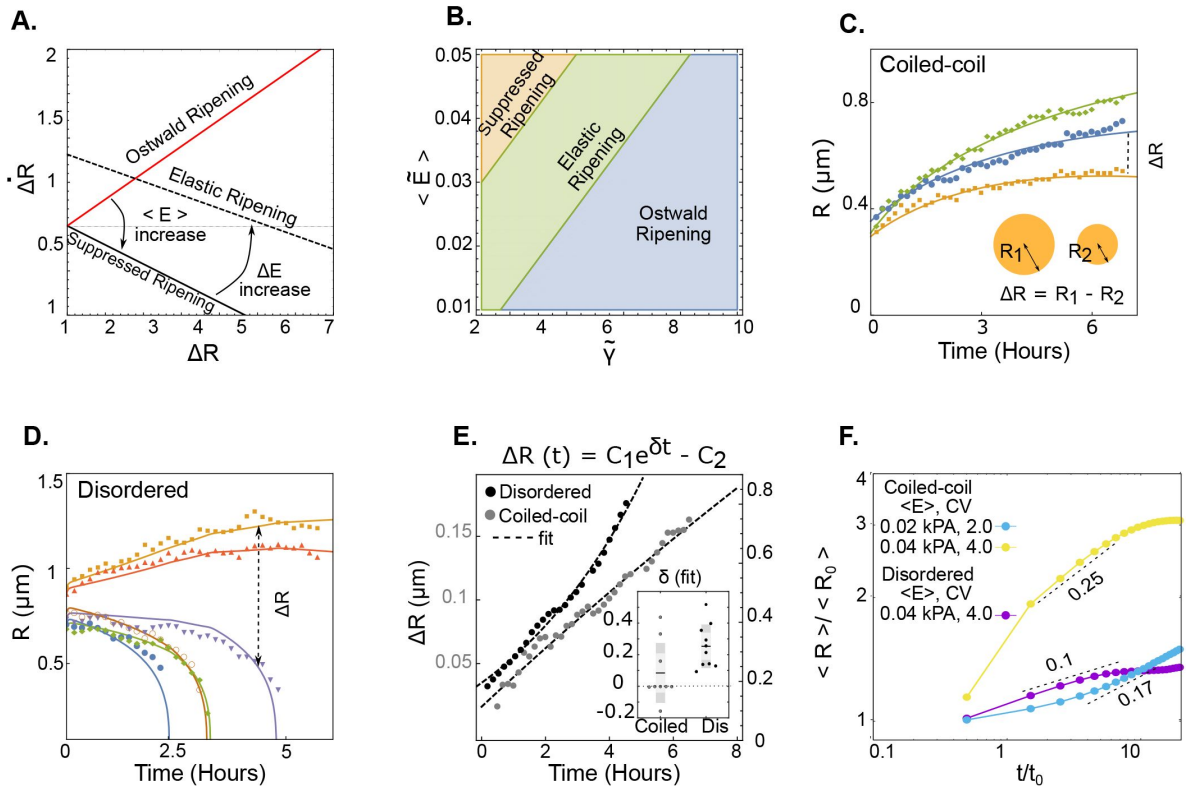

Fig. 3.

Mechanical heterogeneity of the surrounding elastic network induces elastic ripening and slow growth of condensates.

(A) Phase portrait showing the dependence of time-derivative of the condensate size difference, $\dot{\Delta R}$, as a function of Δ*R*. Three distinct growth patterns emerge depending on the slope and the intercept of $\dot{\Delta R}$ vs Δ*R*. (B) Phase diagram in the plane of surface tension $(\tilde{\gamma})$ and mean stiffness $(\langle\tilde{E}\rangle)$ showing the parameter regimes for suppressed ripening, Ostwald ripening and elastic ripening. (C) Time evolution of the sizes of three growing coiled-coil condensates, exhibiting suppressed ripening. Solid lines are model fits to the experimental data. (D) Time evolution of the sizes of five disordered condensates, showing instances of ripening. Solid lines are model fits to the experimental data. (E) Δ*R* vs time for ripening droplets in disordered and coiled-coil condensates show qualitatively distinct trends. (Inset) Characterization of ripening events by obtaining the rate *δ* (in units of hour^{-1}) by fitting linear theory (**Eq. 5**) to experimental data. (F) The numerical solution of the model (**Eq. 4**) for multiple condensates growing in a heterogeneous stiffness landscape predicts power-law scaling of mean condensate sizes during growth. We use high and low values of mean stiffness ($\langle E\rangle$) and coefficient of variation (CV_E) for proteins with low (coiled-coil) and high (disordered) surface tension to predict how different stiffness distributions affect condensate growth. Here $\langle R_0\rangle$ is the mean initial radius of the condensates and the characteristic timescale t_0 = 600 seconds. The parameters used are provided in **Table. 1**.

In a homogeneous elastic medium (i.e., $\Delta E = 0$), the suppression of ripening will result in equal sized condensates ($\Delta R^* = 0$) as has been previously observed (37). Inhomogeneity in the elastic environment will give rise to stable condensates of different sizes (bigger condensates at regions of lower stiffness) and indeed we observe this in the case of suppressed ripening (**Fig. 1H**). Interestingly, This difference in size between the stable condensates (ΔR^*) increases with increasing stiffness difference ΔE and can lead to complete loss of one of the condensates in the stiffer environment when $\Delta R^* \geq R$. We identify this ripening event as elastic ripening driven by the mechanical pressure difference between the condensates due to a difference in their local stiffness values (**Fig. 3A**). In the case of coiled-coil condensates that have very low surface tension, we do observe a few cases of ripening where Ostwald ripening is unlikely (**Fig. 1G,H**). We used **Eq. 5** to predict the phase diagram of the ripening behaviors (at constant $\Delta\tilde{E}$) as a function of $\tilde{\gamma}$ and $\langle\tilde{E}\rangle$ (**Fig. 3B**). The phase diagram shows a transition from Ostwald ripening to elastic ripening and suppressed ripening as surface tension is reduced and stiffness is increased.

We fit our model (**Eq. 4**) to experimental data to gain quantitative insights into the kinetics of condensate growth and ripening (**Fig. 2A**, **Fig. 3C-D**). In particular, the model can also be utilized to infer the mode of ripening (Ostwald vs elastic ripening) directly from the experimental data. The linearized theory predicts that the dynamics of the condensate size difference ΔR evolves in time as

$$\Delta R(t) = (\Delta R(0) + \Delta R^*)e^{\delta t} - \Delta R^* \qquad \textbf{(6)}$$

where $\delta = \frac{2c}{R^3}\left(\tilde{\gamma} - \xi\langle\tilde{E}\rangle/3\right)$. For Ostwald ripening $\delta > 0$ and for elastic ripening (as well as for diffusive growth) $\delta < 0$ (**Fig. 3A**). The quantity ΔR can be easily extracted from the experimental data (**Fig. 3C,D**) and we can fit the time evolution of ΔR to find δ for both coiled-coil and disordered condensates (**Fig. 3E**). Our analysis shows $\delta < 0$ for the majority of the ripening cases in coiled-coil condensates indicating elastic ripening. In contrast, we find that $\delta > 0$ for all of the ripening cases in disordered condensates, indicating Ostwald ripening (**Fig. 3E**-inset). While the theoretical prediction combined with the trend in ΔR data from the experiments indicates elastic ripening in coiled-coil condensates, the magnitudes of the ripening rate δ are small (**Fig. 3E**-inset) such that complete dissolution of coiled-coil condensates is not observed over the experimental timescale (**Fig. 3C**). The slow rate of elastic ripening may result from the smaller values of $\Delta\tilde{E}$, as the coiled coil condensates most likely nucleate in regions of low stiffness in the chromatin network.

Effect of mechanical heterogeneity on condensate nucleation and growth

The chromatin network inside the nucleus is spatially heterogeneous and the local mechanical properties are determined by the local density and the architecture of the chromatin network (38, 39). To understand how heterogeneity in chromatin elasticity affects condensate nucleation and growth, we extended our theory to incorporate the effects of medium elasticity on condensate nucleation. The probability p_{nuc} of nucleating a droplet of size R_0 is given by $p_{\text{nuc}} \propto \exp(-\Delta G/k_B T)$, where ΔG is the free energy change due to nucleation:

$$\Delta G = 4\pi R_0^2 \gamma - \frac{4}{3}\pi R_0^3 \left(c_{\text{in}} k_B T \log S - P_E\right), \qquad \textbf{(7)}$$

with S the extent of super-saturation (see Supplemental Materials Sec. III and Fig. S3). Upon nucleation, the growth dynamics of multiple condensates are given by the system of equations in Eq. 4. The chromatin stiffness landscape is determined by sampling the local stiffness from a normal distribution with mean $\bar{E}$ and coefficient of variation CV_E. We considered a finite pool of

condensate material such that the level of supersaturation S decreases as more condensates are nucleated. Condensate nucleation, growth and coarsening were then studied for different stiffness distributions, for both the coiled-coil and disordered condensates.

In the absence of a surrounding elastic medium, the average condensate size grows in time following the scaling law $\langle R \rangle \sim t^{1/3}$, as expected for coarsening via Ostwald ripening (31, 32). In the presence of an elastic medium, $\langle R \rangle$ does not adhere strictly to a power law scaling over time, but one can fit a power law during the growth phase (**Fig. 3F**). We quantified the scaling behavior of condensate growth with time as, $\langle R \rangle / \langle R_0 \rangle \sim t^{\beta}$, where R_0 is the initial condensate size and β is the scaling exponent. In particular, we computed how β depends on the mean and the variance in stiffness of the surrounding elastic medium, for both coiled-coil and disordered condensates (Fig S4).

We found that the coiled-coil condensates grow faster than the disordered condensates, with β = 0.25 for coiled-coil and β = 0.1 for disordered condensates (**Fig. 3F**), in reasonable quantitative agreement with the experimental data (**Fig. 1L**). Further theoretical analysis predicts that the scaling exponent β decreased with decreasing CV_E and increased with increasing $\bar{E}$ for low surface tension condensates (**Fig. 3F**, Fig S4), while β did not change significantly with stiffness variations for high surface tension condensates (Fig S4). This result contrasts with the known scaling behaviors of condensate coarsening in liquids where the scaling exponent is independent of the properties of the liquid.

Chromatin heterogeneity promotes the growth of low surface tension condensates

To test the model prediction on the effects of chromatin mechanical heterogeneity on the growth of different condensates, we assessed condensate growth in cells with different chromatin environments. First we treated U2OS cells with Trichostatin-A (TSA), a histone deacetylase inhibitor that has been shown to de-condense chromatin and soften the nucleus (40). In addition, we switched cell type to HeLa, which has different nuclei size and chromatin organization. The difference in the chromatin organization in the three types of cells is estimated by differences in the chromatin intensity distribution (**Fig. 4A,B**). HeLa nuclei have significantly greater mean chromatin intensity and variance than untreated U2OS cells, while TSA treatment lowered the chromatin mean intensity and variance in U2OS cells as expected from the de-condensation of chromatin and the resulting increase in the homogeneity of the chromatin environment (**Fig. 4C**, S5A). This suggests both the mean chromatin stiffness and the variance could be different in these three types of cells, reflecting different chromatin environments.

Despite the significant difference in chromatin organization in these nuclei, the growth patterns of the coiled-coil and the disordered condensates remained similar (Fig S5B,E). The coiled-coil condensates still grew mainly by diffusion (73% in TSA treated U2OS cells and 71% in HeLa cells) while the disordered protein condensates grew mostly through ripening (54% in TSA treated U2OS cells, 63% in HeLa cells) (**Fig. 4D,E**). This is consistent with our theoretical results that changes in mean chromatin stiffness or the variance did not impact the pattern of coarsening for coiled-coil and disordered condensates (Fig. S4B). The difference in chromatin environment did not have a significant effect on the growth by fusion for both the condensate types, suggesting that the condensate mobility was similarly limited by chromatin if at all (**Fig. 4D,E**). For the coiled-coil condensates, the reduction of ripening in TSA treated U2OS cells (1.3%) and in HeLa cells (none) is not conclusive due to the scarcity of ripening events (**Fig. 4D**). Comparisons of the ripening time of disordered condensates in the different chromatin environments showed that the chromatin environment did not have a significant impact on ripening dynamics (Fig S5F). These data suggest that condensate growth patterns are dominated by condensate properties and are not significantly affected by physical changes in the chromatin environment.

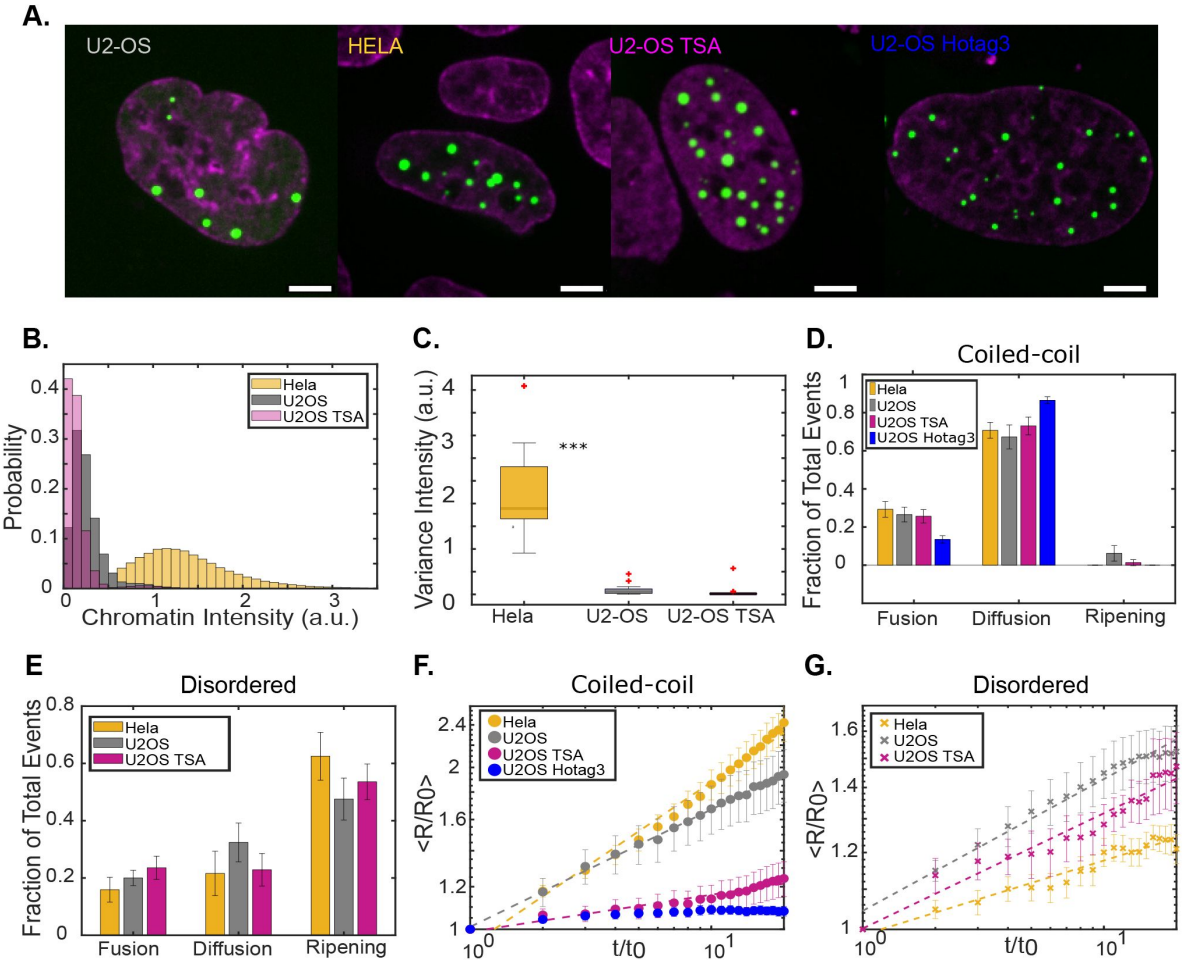

Fig. 4.

Chromatin heterogeneity affects the growth of coiled-coil condensates more than disordered condensates.

(A) Images of representative nuclei (magenta with SPY650DNA staining) with coiled-coil condensates (green) nucleated with LacI in a U2OS cell, a HeLa cell, and a TSA-treated U2OS cell, and that nucleated with Hotag3 in a U2OS cell (scale bar, 5 μm). (B) Distributions of the chromatin intensity for HeLa, U2OS, and TSA treated U2OS cells. (C) The variance of chromatin intensity for HeLa, U2OS, and, TSA treated U2OS cells. (D) Quantification of the growth types of coiled-coil condensates nucleated with LacI in HeLa, U2OS, and TSA treated U2OS cells, and that nucleated with Hotag3 in U2OS cells. (E) Quantification of the growth types of the disordered protein condensates in HeLa, U2OS, and TSA treated U2OS cells. (F) The average radii over time for coiled-coil condensates nucleated with LacI in HeLa, U2OS, TSA treated U2OS cells, and that nucleated with Hotag3 in U2OS cells. (G) The average radii over time for disordered condensates in HeLa, U2OS, TSA treated U2OS cells. In (F) and (G), the radii were normalized to the initial average droplet size by the cell and the time was normalized to the time condensates were nucleated.

However, differences were observed in the condensate growth rates (**Fig. 4F,G**). For coiled-coil condensates, the growth exponent β decreased from 0.22 to 0.07 in TSA treated U2OS cells and increased to 0.3 in HeLa cells, which is still lower than 0.5 predicted by diffusion based growth (29). For disordered condensates, the growth exponent β reduced slightly from 0.14 in untreated cells to 0.12 in TSA treated U2OS cells and 0.08 in HeLa cells (**Fig. 4G**). These trends are consistent with theoretical predictions (Fig S4). Overall, more changes are observed for the coiled-coil condensates and the changes in response to TSA treatment and cell type is different for the two condensates, suggesting that different condensates are affected differently by changes in chromatin landscape.

In addition to the marked difference in the growth exponents, we observed that, after TSA treatment, the average number of condensates formed by the coiled-coil protein significantly increased from 8 condensates per cell to 18 condensates, while the count for the disordered condensates remained similar (8 condensates per cell) (Fig S5G). We hypothesized that TSA treatment may favor coiled-coil condensate nucleation, forming more condensates whose competition for growth quickly quenched available material, resulting in the suppressed growth. To test this hypothesis, we used the stronger nucleator, hexamer Hotag3, that was used for the disordered proteins to induce coiled-coil condensates in untreated U2OS cells (**Fig. 4A**). As expected, more condensates were formed than with the LacI nucleator and the condensate count (19 condensates per cell) was comparable to that in TSA treated cells (Fig S5G), agreeing with the previous findings that condensate nucleation in cells can be modulated by molecular interactions and cellular processes (41). Similar to LacI-induced coiled-coil condensates in various chromatin environments, Hotag3-induced coiled-coil condensates still mainly grow by diffusion (**Fig. 4D**), suggesting that the growth pattern is not sensitive to nucleation. However, these condensates have the smallest growth exponent of 0.02, closer to that in the TSA treated cells (**Fig. 4F**). This suggests that chromatin heterogeneity can control growth dynamics of the low surface tension condensates by affecting nucleation.

Discussion

Nuclear condensates have been previously shown to coarsen primarily via coalescence (29). Here we report that nuclear condensates can coarsen via coalescence, diffusive growth, Ostwald or elastic ripening, and the prevalence of each mode is dictated by the material properties of the condensate. Similar to previously reported suppression of growth in elastic environment (18, 19, 29), we also observed reduced coarsening rates for condensates with different materials. Theoretical modeling shows that different patterns of condensate growth and their coarsening rates result from the interplay between condensate surface tension and chromatin stiffness. This indicates that cells can modulate both condensate properties and chromatin stiffness to regulate condensate growth in the nucleus. After DNA damage, for example, it is known that chromatin is softened and DNA damage proteins undergo multiple types of post-translational modifications (42). It is possible that some of these changes are to regulate chromatin stiffness and condensate properties so that condensate growth at DNA damage sites is favored over other chromatin regions for efficient DNA damage repair.

Many membrane-less compartments need to be stabilized after nucleation. For phase separation to be the driver of the formation of these compartments, an outstanding question has been how do cells prevent Ostwald ripening to achieve compartment stabilization (43). Previous work has shown that internal biochemistry can help prevent Ostwald ripening, which was used to explain centrosome stabilization (8). In addition, for P granules, protein clusters absorbed on the surface can prevent their Ostwald ripening via Pickering stabilization (44). In the human cell nucleus, Ostwald ripening of FUS protein condensates was inhibited by the elastic chromatin (45). By comparing ripening of the two types of condensates in human cell nucleus, our work shows that the elastic chromatin network can stabilize condensates against Ostwald ripening but

only when condensate surface tension is low. This suggests that protein interactions might have been evolved to generate low surface tension condensates to counteract Ostwald ripening. Indeed, there are a wide range of interaction types/strengths from various types of domains/motifs that biological molecules can explore to form condensates (46). Much effort has been focused on how these interactions drive the phase separation process. Our work suggests that understanding how these molecular interactions lead to condensates with different material properties are also important for understanding condensate growth and size control in the nucleus.

By observing condensate growth in different chromatin environments, we discovered that patterns of coarsening show little dependence on the changes in chromatin properties. However, we observed that condensate growth rates are significantly different for different condensates, agreeing with our model prediction that low surface tension condensates grow faster in heterogeneous environments than high surface tension condensates. Interestingly, we also observed noticeable differences in nucleation in different chromatin environment that contributes to the difference in growth dynamics. Previous work has shown that nucleation affects condensate size distribution in cells (47). Our findings imply that nucleation landscape also affects condensate growth kinetics in the nucleus, highlighting the importance of nucleation control for biomolecular condensates. Much like growth, the material properties of condensates could also be significant factors influencing the nucleation landscape within the nucleus. It is possible that cells have adapted to utilize the interaction between chromatin mechanics and condensate properties to regulate nucleation for various biological functions.

Methods

Plasmids

The plasmids used to make the disordered protein condensates were NLS-3xHalo-GFP-Hotag3 and RGG-mCherry-RGG-eDHFR (23, 25, 26). The plasmids used to make the coiled-coil protein condensates were mScarlet-eDHFR-Mad1 as the phase separating protein (26) and Halo-GFP-LacI-NLS as the anchor protein.

Cell culture

The U2OS cells were gifted by Dr. Eros Lazzerini Denchi and the HeLa cells used were recombination-mediated cassette exchange (RMCE) acceptor cells (50). The HeLa cells were cultured in growth medium (Dulbecco's Modified Eagle's medium with 10% FBS and 1% penicillin–streptomycin) and the U2OS cells were cultured in the same media supplemented with 1% glutamine. All cells were cultured at 37 ºC in a humidified atmosphere with 5% CO2. Cells were seeded on 22×22 mm glass coverslips (no. 1.5; Fisher Scientific) coated with poly-D-lysine (Sigma-Aldrich) for transfection at 60 – 70% confluence using Lipofectamine 2000 (ThermoFisher Scientific) according to protocols detailed in published works (23, 25). For the disordered condensate experiments, the cells were co-transfected with 0.5 µg of the NLS-3xHalo-GFP-HoTag3 plasmid DNA and 1 µg of the RGG-mCherry-RGG-eDHFR plasmid. The coiled-coil condensate experiment co-transfections were 0.5 µg of the Halo-GFP-LacI-NLS and 1 µg mScarlet-eDHFR-Mad1. The phase-separating protein and anchor protein combination constructs were thus transiently expressed for 24-48 hours prior to imaging. In the instance of chromatin perturbation, transfected cells (24 hours) were treated with 0.2 mg/ml of Trichostatin-A (TSA, Sigma-Aldrich) for 24 hours before imaging.

Image acquisition and dimerization

For live imaging, the coverslips were mounted into magnetic chambers with 1ml of growth media and 1x SPY650DNA (Spirochrome) as a nuclear stain. Cells without condensates, but with high expression of both the anchor and the phase separating protein were selected and image

acquisition began. At the end of the first time loop, an additional 500 µl of growth media containing the chemical dimerizer TMP-Fluorobenzamide-Halo (TFH) to a final condentration of 100 µM was added to the stage to induce condensate formation in the mounted cells expressing RGG- mCherry-RGG-eDHFR and NLS-3xHalo-GFP-HoTag3 or mScarlet-eDHFR-Mad1 and Halo-GFP-LacI-NLS (23, 25). Z-stack images were collected with 0.6 µm spacing for a total depth of up to 12 µm, at 10 minute intervals for 6-12 hours. A Nikon Eclipse Ti2 microscope with a Tokai Hit stage incubator (with CO2), a Yokogawa CSU-X1 spinning disk confocal equipped with a 100x/1.4 NA oil immersion objective, a XY Piezo-Z stage (Applied Scientific Instrumentation), 488 nm (GFP), 561 nm (mScarlet), and 647 nm (Cy5) laser modules and an EMCCD camera was used to obtain the time lapse images (23, 25).

Image processing

Maximum projections of the z-stack images were pre-processed and the condensates segmented using NIS-Elements Advanced Research Analysis software (5.30.05 64bit, Nikon). The nuclear stain channel (Cy5) was used to isolate nuclear binaries which were tracked and measured using the NIS Elements tracking module. The nuclear binary tracks were then exported to excel spread sheets which were compiled using MATLAB (R2020b, Mathworks) for growth dynamics plots.

Parameter	Numerical value	Source
Protein diffusion constant (D)	$0.01\,\mu\mathrm{m}^2\mathrm{s}^{-1}$	Estimated from fitting parameter b
$c^0_{\mathrm{out}}/c_{\mathrm{in}}$ (Coiled-coil)	0.016	Estimated from partition coefficient (Fig 1)
$c^0_{\mathrm{out}}/c_{\mathrm{in}}$ (Disordered)	0.036	Estimated from partition coefficient (Fig 1)
$\bar{c}/c_{\mathrm{in}}$ (Coiled-coil)	0.0185	Estimated from fitting parameter a
$\bar{c}/c_{\mathrm{in}}$ (Disordered)	0.055	Estimated from fitting parameter a
Supersaturation (Coiled-coil, wild type)	1.007	Calibrated to reproduce measured growth curves
Supersaturation (Coiled-coil, TSA)	1.037	Calibrated
Supersaturation (Disordered, wild type)	1.222	Calibrated
Supersaturation (Disordered, TSA)	1.286	Calibrated
Surface tension (γ) (Coiled-coil)	$10^{-7}\,N\mathrm{m}^{-1}$	This work, (12, 20)
Surface tension (γ) (Disordered)	$10^{-5}\,N\mathrm{m}^{-1}$	This work, (12, 20)
Mesh size	$0.025\,\mu\mathrm{m}$	(48, 49)
Nucleus volume V	$2000\,\mu\mathrm{m}^3$	This work

Table 1.

Parameter values used in numerically solving the model.

Model Fitting

The dynamic equation for droplet growth was reparametrized to fit experimental growth curves. We rewrite Eq. 4 as:

$$\frac{\mathrm{d}R_i}{\mathrm{d}t} = \left[\frac{a}{R_i} - \frac{b}{R_i}\sum_{j=1}^{N} R_j^3 - \frac{c}{R_i}\exp\left(\frac{2\tilde{\gamma}}{R} + \tilde{E}_i g(R)\right)\right] \quad \textbf{(8)}$$

where the renormalized surface tension and stiffness are defined as $\tilde{\gamma} = \gamma/(c_{\mathrm{in}}k_BT)$ and $\tilde{E}_i = E_i/(c_{\mathrm{in}}k_BT)$ respectively. The other parameters are $a = D\bar{c}/c_{\mathrm{in}}$, $b = 4\pi D/3V$, $c = Dc^0_{\mathrm{out}}/c_{\mathrm{in}}$, and $g(R) = \frac{5}{6} - \frac{2\xi_i}{3R_i} - \frac{\xi_i^4}{6R_i^4}$. At room temperature $k_BT \sim 4.114 \times 10^{-21}\,J$ and $c_{\mathrm{in}} \sim 10^5\,\mu m^{-3}$ (51, 52) leading to $c_{\mathrm{in}}k_BT \sim 4 \times 10^{-10}\,N\,\mu m^{-2}$. Depending on the condensate forming protein, the surface tension may be in a range $\sim 10^{-7}$ -$10^{-4}\,Nm^{-1}$ (12, 20) and using the value of $c_{\mathrm{in}}k_BT \sim 4$

$\times 10^{-10} N\,\mu m^{-2}$. Depending on the condensate forming protein, the surface tension may be in a range $\sim 10^{-7}$ –$10^{-4} Nm^{-1}$ (12, 20) and using the value of $c_{in} k_B T \sim 4 \times 10^{-10} N\,\mu m^{-2}$ we can estimate the range of the parameter $\tilde{\gamma} = \gamma/(c_{in} k_B T) \sim 10^{-4} - 10^{-1}\,\mu m$. Using the same value for $c_{in} k_B T$ in a chromatin stiffness range of 1 –1000 Pa (39, 53), the parameter $\tilde{E} = E/(c_{in} k_B T)$ will have values in the range ~0.001 –1.

We estimated the diffusion constant for the dilute phase to be $D = 0.01\,\mu m^2 sec^{-1}$ and obtained the value of parameter c as $D c^0_{out}/c_{in}$ by using the ratio of protein intensities outside and inside the condensate to estimate c^0_{out}/c_{in}. We found the mean value of c^0_{out}/c_{in} to be 0.016 and 0.036 for coiled-coil and disordered proteins, respectively. The mesh size was considered to be $\xi = 0.025\,\mu m$ (48, 49) and the surface tension $\tilde{\gamma}$ was taken to be 0.0001 and 0.01 for the coiled-coil and disordered protein condensates, respectively.

We used a global optimization algorithm *multistart* combined with a nonlinear curve fitting method *lsqcurvefit* in MAT-LAB (54) to find the parameters *a, b* and the local stiffness values $(\tilde{E}_i)$ for each droplet growing in a cell. The algorithm used multiple start points to sample multiple basins of attraction and solve a local optimization to find a set of parameters ({*a, b,* E_i} corresponding to the local start point) that minimized the error $\epsilon = \sum_i \sum_k \left(R(\{a, b, \tilde{E}_i\}, t_k) - R^{i,\text{data}}_k \right)^2$, where $R^{i,\text{data}}(t)$ is the experimentally measured size of the i^{th} condensate at time t and $R(t)$ is the theoretical prediction of i^{th} condensate size obtained from solving Eq. 8 for all condensates in a cell. The sum with index i and k indicate summation over all condensates in a cell and all time points of observation respectively. We used 200– 500 iterations of multi-start to find a convergent trend in the error and considered the fitting parameters corresponding to the smallest ϵ.

Acknowledgements

SB and DC acknowledge support from the National Institutes of Health (NIH R35 GM143042 to SB, GM118510 to DC) and HZ acknowledges support from the National Science Foundation (NSF MCB-2145083). SB, HZ, DB and TC gratefully acknowledge support from the David Scaife Foundation. JK and TC acknowledge support from NIH T32 Fellowship (T32GM133353). TC also acknowledges support from the Brian and Diane Smith Fellowship, GEM Fellowship, CIT Presidential Fellowship, Mahmood I. Bhutta Fellowship.

References

1. Lamond A.I., Sleeman J.E. (2003) **Nuclear substructure and dynamics** *Current Biology* **13**:825–828 https://doi.org/10.1016/j.cub.2003.10.012

2. Mao Y.S., Zhang B., Spector D.L. (2011) **Biogenesis and function of nuclear bodies** *Trends Genet* **27**:295–306 https://doi.org/10.1016/j.tig.2011.05.006

3. Staněk D., Fox A.H. (2017) **Nuclear bodies: news insights into structure and function** *Current Opinion in Cell Biology* **46**:94–101 https://doi.org/10.1016/j.ceb.2017.05.001

4. Brangwynne C.P. (2009) **Germline p granules are liquid droplets that localize by controlled dissolution/condensation** *Science* **324**:1729–1732 https://doi.org/10.1126/science.1172046

5. Hyman A.A., Weber C.A., Jülicher F. (2014) **Liquid-liquid phase separation in biology** *Annual Review of Cell and Developmental Biology* **30**:39–58 https://doi.org/10.1146/annurev-cellbio-100913-013325

6. Banani S.F. (2016) **Compositional control of phase-separated cellular bodies in brief what are the general principles that define the composition of phase-separated cellular bodies?** *Cell* **166**:651–663 https://doi.org/10.1016/j.cell.2016.06.010

7. Strom A.R., Brangwynne C.P. (2019) **The liquid nucleome – phase transitions in the nucleus at a glance** *Journal of Cell Science* **132** https://doi.org/10.1242/jcs.235093

8. Zwicker D., Hyman A.A., Jülicher F. (2015) **Suppression of ostwald ripening in active emulsions** *Physical Review E* **92** https://doi.org/10.1103/PhysRevE.92.012317

9. Dall'Agnese G. (2023) **Role of condensates in modulating dna repair pathways and its implication for chemoresistance** *Journal of Biological Chemistry* **299** https://doi.org/10.1016/j.jbc.2023.104800

10. Zhao R. (2024) **Sumo promotes dna repair protein collaboration to support alterative telomere lengthening in the absence of pml** *bioRxiv* **29** https://doi.org/10.1101/2024.02.29.582813

11. Style Robert W, Sai Tianqi, Nicoló Fanelli, Ijavi Mahdiye, Smith-Mannschott Katrina, Xu Qin, Wilen Lawrence A, Dufresne Eric R (2018) **Liquid-liquid phase separation in an elastic network** *Physical Review X* **8**

12. Zhang Yaojun, Lee Daniel SW, Meir Yigal, Brangwynne Clifford P, Wingreen Ned S (2021) **Mechanical frustration of phase separation in the cell nucleus by chromatin** *Physical Review Letters* **126**

13. Lee Daniel SW, Wingreen Ned S, Brangwynne Clifford P (2021) **Chromatin mechanics dictates subdiffusion and coarsening dynamics of embedded condensates** *Nature Physics* **17**:531–538

14. Huisinga K.L., Brower-Toland B., Elgin S.C.R. (2006) **The contradictory definitions of heterochromatin: transcription and silencing** *Chromosoma* **115**:110–122 https://doi.org/10.1007/s00412-006-0052-x

15. Imai R. (2017) **Density imaging of heterochromatin in live cells using orientation-independent-dic microscopy** *Mol Biol Cell* **28**:3349–3359 https://doi.org/10.1091/mbc.E17-06-0359

16. Constanze B., Cockerill P.N. **Chromatin mechanisms regulating gene expression in health and disease** *Madame Curie Bioscience Database [Internet. Landes Bioscience*

17. Nussinov R. (2023) **Neurodevelopmental disorders, like cancer, are connected to impaired chromatin remodelers, pi3k/mtor, and pak1-regulated mapk** *Biophys Rev* **15**:163–181 https://doi.org/10.1007/s12551-023-01054-9

18. Style R.W. (2018) **Liquid-liquid phase separation in an elastic network** *Physical Review X* **8** https://doi.org/10.1103/PHYSREVX.8.011028

19. Rosowski K.A., Vidal-Henriquez E., Zwicker D., Style R.W., Dufresne E.R. (2020) **Elastic stresses reverse ostwald ripening †** *Soft Matter* **16** https://doi.org/10.1039/d0sm00628a

20. Wang H., Kelley F.M., Milovanovic D., Schuster B.S., Shi Z. (2021) **Surface tension and viscosity of protein condensates quantified by micropipette aspiration** *Biophysical Reports* **1** https://doi.org/10.1016/j.bpr.2021.100011

21. Wan J. (2019) **Mad1 destabilizes p53 by preventing pml from sequestering mdm2** *Nat Commun* **10** https://doi.org/10.1038/s41467-019-09471-9

22. Elbaum-Garfinkle S. (2015) **The disordered p granule protein laf-1 drives phase separation into droplets with tunable viscosity and dynamics** *Proceedings of the National Academy of Sciences* **112**:7189–7194 https://doi.org/10.1073/PNAS.1504822112

23. Zhang H. (2020) **Nuclear body phase separation drives telomere clustering in alt cancer cells** *Molecular Biology of the Cell* :19–10 https://doi.org/10.1091/mbc.e19-10-0589

24. Zhao C., Chenoweth R.M., Zhang D.M. (2021) **Chemical dimerization-induced protein condensates on telomeres** *J. Vis. Exp* https://doi.org/10.3791/62173

25. Lackner R.M., O'Connell W., Zhang H., Chenoweth D.M. (2022) **A general strategy for the design and evaluation of heterobifunctional tools: Applications to protein localization and phase separation** *Chembiochem* **23** https://doi.org/10.1002/cbic.202200209

26. Zhang H., Aonbangkhen C., Tarasovetc E.V., Ballister E.R., Chenoweth D.M., Lampson M.A. (2017) **Optogenetic control of kinetochore function** *Nature Chemical Biology* **13**:1096–1101 https://doi.org/10.1038/nchembio.2456

27. Wang Z., Lou J., Zhang H. (2022) **Essence determines phenomenon: Assaying the material properties of biological condensates** *Journal of Biological Chemistry* **298** https://doi.org/10.1016/J.JBC.2022.101782

28. Huaiying Zhang (2015) **Rna controls polyq protein phase transitions** *Molecular cell* **60**:220–230 https://doi.org/10.1016/J.MOLCEL.2015.09.017

29. Lee D.S.W., Wingreen N.S., Brangwynne C.P. (2021) **Chromatin mechanics dictates subdiffusion and coarsening dynamics of embedded condensates** *Nat. Phys* **17** https://doi.org/10.1038/s41567-020-01125-8

30. Berry J., Weber S.C., Vaidya N., Haataja M., Brangwynne C.P. (2015) **Rna transcription modulates phase transition-driven nuclear body assembly** *Proceedings of the National Academy of Sciences* **112**:5237–5245 https://doi.org/10.1073/pnas.1509317112

31. Lifshitz Ilya M, Slyozov Vitaly V (1961) **The kinetics of precipitation from supersaturated solid solutions** *Journal of physics and chemistry of solids* **19**:35–50

32. Wagner Carl (1961) **Theorie der alterung von niederschlägen durch umlösen (ostwald-reifung)** *Zeitschrift für Elektrochemie, Berichte der Bunsengesellschaft für physikalische Chemie* **65**:581–591

33. Voorhees Peter W (1985) **The theory of ostwald ripening** *Journal of Statistical Physics* **38**:231–252

34. Ghosh Soham, Seelbinder Benjamin, Henderson Jonathan T, Watts Ryan D, Scott Adrienne K, Veress Alexander I, Neu Corey P (2019) **Deformation microscopy for dynamic intracellular and intranuclear mapping of mechanics with high spatiotemporal resolution** *Cell reports* **27**:1607–1620

35. Heo Su-Jin *et al.* (2020) **Nuclear softening expedites interstitial cell migration in fibrous networks and dense connective tissues** *Science advances* **6**

36. Gent AN, Lindley PB (1959) **Internal rupture of bonded rubber cylinders in tension** *Proceedings of the Royal Society of London. Series A. Mathematical and Physical Sciences* **249**:195–205

37. Rosowski Kathryn A, Sai Tianqi, Vidal-Henriquez Estefania, Zwicker David, Style Robert W, Dufresne Eric R (2020) **Elastic ripening and inhibition of liquid–liquid phase separation** *Nature physics* **16**:422–425

38. Misteli T. (2020) **The self-organizing genome: Principles of genome architecture and function** *Cell* **183**:28–45 https://doi.org/10.1016/j.cell.2020.09.014

39. Vivante Anat, Bronshtein Irena, Garini Yuval (2020) **Chromatin viscoelasticity measured by local dynamic analysis** *Biophysical journal* **118**:2258–2267

40. Stephens A.D. (2018) **Chromatin histone modifications and rigidity affect nuclear morphology independent of lamins** *Molecular Biology of the Cell* **29**:220–233 https://doi.org/10.1091/MBC.E17-06-0410

41. Shimobayashi S.F., Ronceray P., Sanders D.W., Haataja M.P., Brangwynne C.P. (2021) **Nucleation landscape of biomolecular condensates** *Nature* https://doi.org/10.1038/s41586-021-03905-5

42. Santos Á. (2020) **Dna damage alters nuclear mechanics through chromatin reorganization** *Nucleic Acids Res* **49**:340–353 https://doi.org/10.1093/nar/gkaa1202

43. Snead W.T., Gladfelter A.S. (2019) **The control centers of biomolecular phase separation: How membrane surfaces, ptms, and active processes regulate condensation** *Molecular Cell* **76**:295–305 https://doi.org/10.1016/J.MOLCEL.2019.09.016

44. Folkmann A.W., Putnam A., Lee C.F., Seydoux G. (2021) **Regulation of biomolecular condensates by interfacial protein clusters** *Science* **373**:1218–1224 https://doi.org/10.1126/science.abg7071

45. Zhang Y., Lee D.S.W., Meir Y., Brangwynne C.P., Wingreen N.S. (2021) **Mechanical frustration of phase separation in the cell nucleus by chromatin** *Physical review letters* **126** https://doi.org/10.1103/PHYSREVLETT.126.258102

46. Brangwynne C.P., Tompa P., Pappu R.V. (2015) **Polymer physics of intracellular phase transitions** *Nature Physics* **11**:899–904 https://doi.org/10.1038/nphys3532

47. Lee D.S.W. (2023) **Size distributions of intracellular condensates reflect competition between coalescence and nucleation** *Nature Physics* :1–11 https://doi.org/10.1038/s41567-022-01917-0

48. Solovei Irina, Cavallo Antonio, Schermelleh Lothar, Jaunin Françoise, Scasselati Catia, Cmarko Dusan, Cremer Christoph, Fakan Stanislav, Cremer Thomas (2002) **Spatial preservation of nuclear chromatin architecture during three-dimensional fluorescence in situ hybridization (3d-fish)** *Experimental cell research* **276**:10–23

49. Görisch Sabine M, Richter Karsten, Scheuermann Markus O, Herrmann Harald, Lichter Peter (2003) **Diffusion-limited compartmentalization of mammalian cell nuclei assessed by microinjected macromolecules** *Experimental cell research* **289**:282–294

50. Khandelia P., Yap K., Makeyev E.V. (2011) **Streamlined platform for short hairpin rna interference and transgenesis in cultured mammalian cells** *Proceedings of the National Academy of Sciences of the United States of America* **108**:12799–12804 https://doi.org/10.1073/PNAS.1103532108

51. Bracha Dan, Walls Mackenzie T, Wei Ming-Tzo, Zhu Lian, Kurian Martin, Avalos José L, Toettcher Jared E, Brangwynne Clifford P (2018) **Mapping local and global liquid phase behavior in living cells using photo-oligomerizable seeds** *Cell* **175**:1467–1480

52. Wei Ming-Tzo, Elbaum-Garfinkle Shana, Holehouse Alex S, Carlos Chih-Hsiung Chen, Feric Marina, Arnold Craig B, Priestley Rodney D, Pappu Rohit V, Brangwynne Clifford P (2017) **Phase behaviour of disordered proteins underlying low density and high permeability of liquid organelles** *Nature chemistry* **9**:1118–1125

53. Shin Yongdae, Chang Yi-Che, Lee Daniel SW, Berry Joel, Sanders David W, Ronceray Pierre, Wingreen Ned S, Haataja Mikko, Brangwynne Clifford P (2018) **Liquid nuclear condensates mechanically sense and restructure the genome** *Cell* **175**:1481–1491

54. The MathWorks Inc (2022) **Matlab**

Author information

Deb Sankar Banerjee*

Department of Physics, Carnegie Mellon University, Pittsburgh, PA 15213, USA, James Franck Institute, University of Chicago, Chicago, USA

*These authors contributed equally to this work

Tafadzwa Chigumira*
Department of Chemical Engineering, Carnegie Mellon University, Pittsburgh, USA

*These authors contributed equally to this work

Rachel M Lackner
Department of Chemistry, University of Pennsylvania, Philadelphia, USA

Josiah C Kratz
Department of Biological Sciences, Carnegie Mellon University, Pittsburgh, USA, Computational Biology Department, Carnegie Mellon University, Pittsburgh, USA

David M Chenoweth
Department of Chemistry, University of Pennsylvania, Philadelphia, USA

Shiladitya Banerjee
Department of Physics, Carnegie Mellon University, Pittsburgh, PA 15213, USA

For correspondence: shiladtb@andrew.cmu.edu

Huaiying Zhang
Department of Chemical Engineering, Carnegie Mellon University, Pittsburgh, USA, Department of Biological Sciences, Carnegie Mellon University, Pittsburgh, USA
ORCID iD: 0000-0002-1784-2664

For correspondence: huaiyinz@andrew.cmu.edu

Editors

Reviewing Editor
Qiang Cui
Boston University, Boston, United States of America

Senior Editor
Qiang Cui
Boston University, Boston, United States of America

Reviewer #1 (Public review):

Summary:

The manuscript "Interplay of condensate material properties and chromatin heterogeneity governs nuclear condensate ripening" presents experiments and theory to explain the dynamic behavior of nuclear condensates. The authors present experimental data that shows the size of multiple artificially induced condensates as a function of time for various conditions. They identify different dynamic regimes, which all differ from traditional Ostwald ripening. By careful analysis and comparison with a quantitative model, the authors conclude that the elastic effects of the chromatin are relevant and the interplay between (heterogeneous) elasticity and surface tension governs the droplets' behavior. However, since

they apply a simple model to a complex system, I think that the work is sometimes prone to over-interpretation, which I detail below. In summary, since droplet growth in a heterogeneous, elastic environment is unavoidable for condensates, this work achieves an important step toward understanding this complex setting. The work will likely stimulate more experiments (using different methods or alternative settings) as well as theory (accounting for additional effects, like spatial correlations).

Strengths:

A particularly strong point of the work is the tight integration between experiment and theory. Both parts are explained well at an appropriate level with more details in the methods section and the supplementary information. I cannot comment much on the experiments, but they seem convincing to me and the authors quantify the relevant parameters. Concerning the theory, they derive a model at the appropriate level of description. The analysis of the model is performed and explained well. Even though spatial correlations are not taken into account, the model will serve as a useful basis for developing more complicated models in the future. It is also worth mentioning that the clear classification into different growth regimes is helpful since such results, with qualitative predictions for parameter dependencies, likely also hold in more complex scenarios.

Weaknesses:

I think that the manuscript would profit from more precise definitions and explanations in multiple points, as detailed below. Clearly, not all these points can be fully incorporated in a model at this point, but I think it would be helpful to mention weaknesses in the manuscript and to discuss the results a bit more carefully.

(1) The viscosity analysis likely over-interprets the data. First, the FRAP curves do not show clear exponential behavior. For Figure 1C, there are at least two time scales and it is not clear to me why the shorter time scale right after bleaching is not analyzed. If the measured time scale were based on the early recovery, the differences between the two cases would likely be very small. For Figure 1D, the recovery is marginal, so it is not clear how reliable the measurements are. More generally, the analysis was performed on condensates of very different sizes, which can surely affect the measurements; see https://doi.org/10.7554/eLife.68620 for many details on using FRAP to analyze condensate dynamics. Second, the relaxation dynamics are likely not purely diffusive in a viscous environment since many condensates show elastic properties (https://doi.org/10.1126/science.aaw4951). I could very well imagine that the measured recovery time is related to the viscoelastic time scale. Third, the assumption of the Stokes-Einstein-Sutherland equation to relate diffusivity and viscosity is questionable because of viscoelasticity and the fact that the material is clearly interacting, so free diffusion is probably not expected.

(2) A large part of the paper is spent on the difference between different dynamic regimes, which are called "fusion", "ripening", and "diffusion-based" (with slightly different wording in different parts). First, I would welcome consistent language, e.g., using either fusion or coalescence. Second, I would welcome an early, unambiguous definition of the regimes. A definition is given at the end of page 2, but this definition is not clear to me: Does the definition pertain to entire experiments (e.g., is something called "fusion" if any condensates fuse at any time in the experiment?), or are these labels used for different parts of the experiment (e.g., would the data in Figure 1H first be classified as "ripening" and then "diffusion-based")? More generally, the categorization seems to depend on the observed system size (or condensate count) and time scale. Third, I find the definition of the ripening time a bit strange since it is clearly correlated with droplet size. Is this dependency carefully analyzed in the subsequent parts?

(3) The effect of the elastic properties of the chromatin is described by a Neo-Hookean model, but the strains R/\xi used in the theory are of the order of 100, which is huge. At such high strains, the Neo-Hookean model essentially has a constant pressure 5E/6, so the mesh size \xi does not matter. It is not clear to me whether chromatin actually exhibits such behavior, and I find it curious that the authors varied the stiffness E but not the mesh size \xi when explaining the experiments in the last section although likely both parameters are affected by the experimental perturbations. In any case, https://doi.org/10.1073/pnas.2102014118 shows that non-linear elastic effects related to breakage and cavitation could set in, which might also be relevant to the problem described here. In particular, the nucleation barrier discussed in the later part of the present manuscript might actually be a cavitation barrier due to elastic confinement. In any case, I would welcome a more thorough discussion of these aspects (in particular the large strains).

(4) The description of nucleation on page 7 is sloppy and might be misleading. First, at first reading I understood the text as if droplets of any radius could nucleate with probability p_nuc related to Eq. 7. This must be wrong since large droplets have $\Delta G<0$ implying p_nuc > 1. Most likely, the nucleation rate only pertains to the critical radius (which is what might be meant by R_0, but it is unclear from the description). In this case, the critical radius and its dependence on parameters should probably be discussed. It might also help to give the value of the supersaturation S in terms of the involved concentrations, and it should be clarified whether P_E depends on R_0 or not (this might also relate to the cavitation barrier raised in point 3 above). Secondly, it is a bit problematic that E is sampled from a normal distribution, which allows for negative stiffnesses! More importantly, the exact sampling protocol is important since sampling more frequently (in the simulations) leads to a larger chance of hitting a soft surrounding, which facilitates nucleation. I could not find any details on the sampling in the numerical simulations, but I am convinced that it is a crucial aspect. I did find a graphical representation of the situation in Figure S4A, but I think it is misleading since there is no explicit space in the model and stiffnesses are not correlated.

https://doi.org/10.7554/eLife.101777.1.sa1

Reviewer #2 (Public review):

Summary:

The authors used a chemical linker to induce phase separation in U2OS cell nuclei with two different proteins, a coiled-coil protein (Mad1) and a disordered domain (from LAF-1), whose condensates were purported to have different material properties. First, they performed Fluorescence Recovery After Photobleaching (FRAP) and estimated the viscosity via the Stokes-Einstein equation. Combined with droplet fusion assays, this yielded an estimate of the surface tension, wherein the disordered condensates were found to have 130 times higher surface tension than the coiled-coil condensates. Confocal fluorescence microscopy was used to follow condensates over time, enabling classification of growth events as either fusion-, ripening-, or diffusion-based, and subsequent comparison of the relative abundances of these growth events between the two condensate types. Coiled-coil condensates grew primarily by diffusive processes, whereas disordered condensates grew primarily by ripening processes. The coarsening rates were described by growth exponents extracted from power-law fits of average normalized condensate radius over time. In both cases, these growth exponents were smaller than those predicted by theory, leading the authors to propose that nuclear condensate growth is generally suppressed by chromatin mechanics, as found in previous studies albeit with different exponents. The authors developed a theory to understand how the extent of this effect may depend on condensate material properties like surface tension. Treating chromatin as a neo-Hookean elastic solid, the authors assume a form of mechanical pressure that plateaus with increasing condensate size, and the resulting theory is used to

analyze the observed condensate growth dynamics. A linearized extension of the theory is used to distinguish between suppressed, elastic, and Ostwald ripening. Finally, the authors consider the impact of different chromatin environments on condensate growth patterns and dynamics, which is achieved experimentally with another cell type (HeLa) and with a drug that decondenses chromatin (TSA). They find that condensate growth patterns are not significantly changed in either condensate type, but that the number of condensates nucleated and their related growth exponent are more sensitive to variations in chromatin stiffness in the coiled-coil system due to its low surface tension.

Strengths:

This work provides evidence that nuclear condensates can coarsen not only by fusion but also by continuous diffusive growth processes, predominant in coiled-coil condensates, and ripening, predominant in disordered condensates. Across these different condensate types and coarsening mechanisms, the authors find growth exponents lower than theoretical expectations, reinforcing the notion that elastic media can suppress condensate growth in the nucleus. Combined with theory, these observed differences in growth patterns and rates are argued to originate from differences in material properties, namely, surface tension relative to local chromatin stiffness. The authors further suggest that the few ripening events that are seen in coiled-coil condensates may be elastic in nature due to gradients in chromatin stiffness as opposed to Ostwald ripening. If this assertion proves to be robust, it would mark an early observation of elastic ripening in living cells.

Weaknesses:

(1) The assertion that nuclear condensates experience an external pressure from the chromatin network implies that chromatin should be excluded from the condensates (Nott et al., Molecular Cell (2015); Shin et al., Cell (2018)). This has not been shown or discussed here. While Movie 1 suggests the coiled-coil condensates may exclude chromatin, Movie 2 suggests the disordered condensates do not. LAF-1, as an RNA helicase, interacts with RNA, and RNA can be associated with chromatin in the nucleus. RNA can also modulate droplet viscosity. The authors' analysis of the disordered condensate data only makes sense if these condensates exclude chromatin, which they have not demonstrated, and which appears not to be the case.

(2) Critical physical parameters like viscosity and surface tension have not been directly measured but rather are estimated indirectly using FRAP and the Stokes-Einstein equation. While not uncommon in the field, this approach is flawed as droplet viscosity is not simply determined by the size of the composing particles. Rather, in polymeric systems, viscosity strongly depends on the local protein concentration and intermolecular interactions (Rubinstein & Semenov Macromolecules (2001)). This unjustified approach propagates to the surface tension estimate since only the ratio of viscosity to surface tension is explicitly measured. Since the paper's conclusions strongly hinge on the magnitude of the surface tension, a more accurate estimate or direct measurement of this salient material property is called for.

(3) The phase diagram of growth modes very much depends on the assumption of neo-Hookean elasticity of the chromatin network. This assumption is poorly justified and calls into question the general conclusions about possible growth phases. The authors need to either provide evidence for neo-Hookean elasticity, or, alternatively, consider a model in which strain stiffening or thinning continues as droplets grow, which would likely lead to very different conclusions, and acknowledge this uncertainty.

(4) There is limited data for the elastic ripening claim. In Figure 3E, only one data point resides in the elastic ripening ($\delta < 0$) range, with a few data points very close to zero.

(5) The authors claim that "our work shows that the elastic chromatin network can stabilize condensates against Ostwald ripening but only when condensate surface tension is low." This claim also depends on the details of the chosen neo-Hookean model of chromatic elasticity, and it is not studied here whether these results are robust to other models.

(6) It is also not clear how the total number of Mad1 proteins and LAF-1 disordered regions change while the condensates evolve with time. As the experiments span longer than 6 hours, continued protein production could lead to altered condensate coarsening dynamics. For example, continued production of Mad1 can lead to the growth of all Mad1 condensates, mimicking the diffusive growth process.

https://doi.org/10.7554/eLife.101777.1.sa0

Author response:

We appreciate the reviewer's recognition of the strengths of our work as well as their constructive critiques and insightful suggestions for improvement. In this provisional response, we outline how we plan to address the reviewer's comments in the revised manuscript.

(1) Viscosity and surface tension are not accurately measured.

We thank the reviewers for bringing up this important point. We are aware that FRAP is not the best method to accurately measure condensate viscoelasticity due to the problems the reviewers and others in the field have pointed out. More accurate methods of measuring fluorescent protein mobility, such as single-molecule tracking or fluorescence correlation spectroscopy, can be used; however, they cannot accurately reflect the time scale dependence of viscoelasticity in the condensate either. Other methods such as rheology and micropipette aspiration that have been used to measure condensate viscoelasticity in vitro are not accessible in living cells yet. Similarly, there is no readily available method to directly measure the surface tension of condensates in live cells. Therefore, we used FRAP and fusion assays to estimate the ratio of surface tension between the two condensates. This ratio was then used to determine the surface tension of the coiled coil condensates in the model after estimating the surface tension for disordered condensate from in vitro measurements (https://doi.org/10.1016/j.bpr.2021.100011). In the revision, we will adjust our FRAP fitting and use condensates with similar sizes to make our FRAP data more accurate. However, based on the large difference we observed for these two condensates, we do not believe these FRAP improvements would change the conclusions.

We are also aware that the stokes-einstein relation strictly applies to purely viscous systems. One can apply the generalized Stokes-Einstein relation, which links the diffusion coefficient to the complex viscoelastic modulus of the medium. However, the complex modulus is difficult to determine in cells through live imaging. We thus used the Stokes-Einstein relation to estimate the ratio of effective viscosities, assuming elastic deformations relax faster. In the revision, we will add these assumptions to our discussion.

(2) Justification of a Neo-Hookean elasticity model for chromatin.

We thank the reviewer for highlighting this important aspect of our work. The observation that the strains R/ξ in our initial model are of the order of 100 is valid and raises questions about the applicability of the Neo-Hookean model. While it is true that at such high strains, the pressure becomes nearly constant (5E/6), our model remains applicable within the range of strains relevant to chromatin, particularly for small droplets where R/ξ values are more moderate. This is explicitly considered in the section "Effect of mechanical heterogeneity on condensate nucleation and growth," where we also account for heterogeneous mesh sizes

correlated with local stiffness. While these points are discussed in the supplementary material, we acknowledge that these details are not clearly presented in the main text, and we will revise the manuscript to explicitly discuss the strain regime and model applicability.

We agree that varying both the stiffness E and mesh size ξ would provide a more comprehensive understanding of the system, as both parameters are likely affected by experimental perturbations. We will revisit our analysis to incorporate variations in ξ alongside E and discuss the potential effects on our results.

Furthermore, the stabilization of condensate size by chromatin elasticity arises from the size-dependent pressure exerted by the elastic network, which is a feature of strain-stiffening elastic media rather than a specific property of the Neo-Hookean model. However, we agree that exploring the robustness of our results under alternative elasticity models would strengthen the manuscript. In the revised version, we will analyze additional elasticity models, including strain stiffening and thinning, to evaluate how these might influence our conclusions and to provide a broader context for the predicted growth phases.

The connection between the nucleation barrier and the cavitation barrier is particularly intriguing. The referenced study (https://doi.org/10.1073/pnas.2102014118) highlights non-linear elastic effects, including breakage and cavitation, which may be relevant in our system. We will explore whether cavitation effects due to elastic confinement play a role in the nucleation dynamics observed here and include a discussion of these mechanisms in the revised manuscript.

(3) Unclear description of nucleation in the model.

We thank the reviewer for pointing out the lack of clarity in our description of nucleation. R_0 represents the critical radius for nucleation, beyond which droplets grow spontaneously. The nucleation probability p_nuc is evaluated at R_0, which depends on the free energy barrier ΔG, supersaturation S, and the elastic properties of the surrounding medium. We will include a clearer explanation of R_0, its dependence on parameters, and its role in nucleation in the revised manuscript.

We ensure that the stiffness is sampled from a truncated normal distribution, preventing negative stiffness values. Sampling is performed at fixed intervals, and we will clarify the protocol to avoid bias and ensure consistency in the simulations.

Supersaturation S will be defined regarding solute and solvent concentrations, and we will discuss its influence on ΔG and R_0.

The dependence of the elastic pressure P_E on R_0, with stiffer surroundings leading to smaller nucleated droplets, will be explicitly clarified. We also agree that Figure S4A may be misleading, as it suggests spatial correlations in stiffness. We will revise the figure and caption to better represent the model assumptions.

(4) Limited data for the elastic ripening claim.

We acknowledge the reviewer's concern regarding the limitation of support for the claim in the current manuscript. We believe our data do indicate elastic ripening. Particularly, the data points very close to zero are not necessarily artifacts of the fitting, as the elastic ripening can be very slow due to small differences in the local stiffness values around the droplets. We have mentioned this at the end of the section "Condensate material properties and chromatin heterogeneity determine the modes of ripening". We shall revisit these results and remedy this concern with more data and analysis in the revised manuscript.

(5) Confusion for dynamic regimes such as "fusion", "ripening", and "diffusion-based" and the problem with using "ripening time" to compare ripening speed.

We will clear up our definitions of the dynamic regimes and ensure consistent language use. The ripening time was defined as the time it takes per length of droplets to shrink. This way, the size dependence of the absolute ripening time is decoupled and thus can be used to compare the speed of ripening between two condensates. This is not well-explained in our current version. In the revision, we will redefine the normalized ripening time to avoid this confusion.

(6) Chromatin should be excluded from the condensates

We have data to support that chromatin is excluded from the condensates. We will add the data in the revision.

(7) Effect of protein production on the diffusive growth process.

From the experiment, we do not believe that protein production is a significant source of the diffusive growth because for coiled-coil condensates nucleated with Hotag3 there was little diffusive growth. In the model also, condensates can grow for hours in the absence of protein production, depending on chromatin stiffness and surface tension. We aim to address the effect of protein production on growth in the revised manuscript.

https://doi.org/10.7554/eLife.101777.1.sa3